Studies on the Reduction of $[(C_5Me_5)_2Mo_2O_5]$ in Methanol/Water/Acetate Solutions by On-Line Electrochemical Flowcell and Electrospray Mass Spectrometry

Jenny Gun,*[a] Alexandre Modestov,[a] Ovadia Lev,[a] Dirk Saurenz,[b] Mikhail A. Vorotyntsev,[b] and Rinaldo Poli*[b]

Keywords: Cyclopentadienyl ligands / Electrochemistry / Mass spectrometry / Molybdenum / Oxo ligands

The complex $[Cp^*_2Mo_2O_5]$ ($Cp^* = \eta^5$-C_5Me_5) and its electrochemical reduction products in acetic acid/acetate-buffered (pH = 4.0) water/methanol solutions were investigated by combined electrochemical (EC) flowcell and on-line electrospray ionization mass spectrometry (ESI-MS). Mono-, di-, tri-, and tetranuclear organometallic molybdenum oxides were identified in the starting solution. The effect of the relevant ESI-MS parameters (ionic mode, heated capillary voltage, and heated capillary temperature) and of the concentration on the observed distribution of ions in the mass spectrometer was studied in order to minimize side reactions in the ESI chamber. It was verified that reduction in the ESI-MS is undetectable under open-circuit conditions. The on-line electrochemical study revealed the potential-dependent formation of previously unknown mono-, di-, tri-, and tetranuclear Mo^V, Mo^{IV}, and mixed-valence complexes. The compounds were identified by their characteristic isotope patterns and their ion trap MS^n fragmentations. The observed formation potentials reflect the higher stability of the multinuclear species relative to the mononuclear ones with the same oxidation state.

Introduction

The rapid development and eventual commercialization of Electrospray Ionization Mass Spectrometers (ESI-MS) in the 1980s and 1990s has opened the door to the determination of nonvolatile inorganic, organic, and organometallic compounds by mass spectrometry.[1,2] ESI-MS is an atmospheric-pressure technique that uses an electrostatic sprayer to transfer ionic solutes from the sample solution to the gas phase.[3,4] The ESI-MS technique is gradually becoming a valuable tool for the investigation of organometallic compounds in both protic and aprotic solvents[4] and has proven especially useful in combination with investigations of redox processes, particularly reduction processes.

Electrochemical methods are the method of choice for obtaining reduced organometallic compounds, since potential-dependent information can readily be obtained, reversibility is easily checked, and complexation by the chemical reducing agents or their by-products is minimized. Bond et al. have made extensive use of ESI-MS for the investigation of complex electrochemical transformations of organometallic compounds such as the reductions of *cis*-$[(Et_2\text{-dcbpy})_2RuX_2]$ (X = Cl^-, I^-, NCS^-, CN^-)[5] and 17-electron carbonyl(phosphane)rhenium(II) complexes.[6] These works are based on the combination of preparative electrochemistry and subsequent ESI-MS analysis. However, preparative electrochemistry suffers from several disadvantages. Firstly, considerable time is needed in order to achieve full conversion, thereby limiting the resolution of potential-dependent investigations. Secondly, the long reduction times often involve fouling of the electrode surface by polymeric by-products. Thirdly, the reduced compounds have ample time to participate in unwanted subsequent chemical reactions among themselves or with the oxidized forms. Fourthly, preparative electrochemistry monitored by ESI-MS studies involves considerable sample handling, which may result in oxygen penetration and impurity introduction.

The importance of flow-through electrochemical cells connected to a mass spectrometer and the instrumentation involved have recently been reviewed.[7] Cole et al.,[8,9] Bond et al.,[10] and Van Berkel et al.,[11,12] used different configurations of electrochemical cells coupled to on-line ESI mass spectrometers for the investigation of redox reactions. We have devised an on-line concentric electrochemical cell

[a] Laboratory of Environmental Chemistry, Division of Environmental Sciences and The Casali Institute, The Hebrew University of Jerusalem
Jerusalem, Israel
Fax: (internat.) + 972-2/658-6155
E-mail: gunjen@pob.huji.ac.il
[b] Laboratoire de Synthèse et d'Electrosynthèse Organométalliques, Faculté des Sciences "Gabriel", Université de Bourgogne,
6 Boulevard Gabriel, 21000 Dijon, France
Fax: (internat.) + 33-3/80393720
E-mail: poli@u-bouregogne.fr

connected to ESI-MS in which the counter-electrode and its products are separated from the reacting stream reaching the ESI-MS in order to isolate and protect the reduced compounds from the oxidized substances generated at the counter-electrode.

Oxygen-containing organomolybdenum complexes are especially intriguing since, in spite of their ability to attain a large number of oxidation states, relatively little is known about their speciation in protic solutions or about their electrochemistry. More information, on the other hand, is available on inorganic oxomolybdenum compounds, including ESI-MS speciation studies. Singly, doubly, and triply charged heteropoly- and isopolymolybdate anions were studied in organic and aqueous organic solutions,[13,14] though the reduction products of these compounds were not investigated by mass spectrometry. The subject of this study is the identification of the electrochemical reduction products of the complex $[Cp^*_2Mo_2O_5]$ in aqueous methanol solution. $[Cp^*_2Mo_2O_5]$ is a member of a relatively broad family of high-oxidation organometallic compounds, some of which have displayed some remarkable stoichiometric and/or catalytic chemical transformations. Although some of these molecules are stable in aqueous environments and have even been synthesized in water, their aqueous chemistry has rarely been investigated. In the particular case of $[Cp^*_2Mo_2O_5]$, while most studies have been carried out in organic solvents,[15−19] other contributions have restricted the use of aqueous media to some aspects of the synthetic procedure.[20−23] Some of us have recently reported an improved aqueous synthesis[24] of $[Cp^*_2Mo_2O_5]$ and a detailed investigation of its speciation in a $MeOH/H_2O$ mixture by conductivity studies.[25] An additional point of interest of this molybdenum system is the redox-richness of the metal. Exploration of the redox behavior of $[Cp^*_2Mo_2O_5]$ as a prototype compound may thus open up avenues for the development of new stoichiometric or catalytic redox chemistry.

Results and Discussion

(a) Studies of $[Cp^*_2Mo_2O_5]$ Solutions and Optimization of ESI-MS Conditions

The speciation of $[Cp^*_2Mo_2O_5]$ in water/methanol mixtures at various pH values is known from recent kinetic and conductivity studies in one of our laboratories.[25] The use of a mixed water/methanol medium was dictated by the insolubility of $[Cp^*_2Mo_2O_5]$ in pure water, while the hydrosoluble (but lipophobic) $[Cp^*MoO_3^-]$ ion is obtained under basic conditions. As a brief summary of the speciation studies, compound $[Cp^*_2Mo_2O_5]$ was found to exist as a dinuclear molecular species in organic solvents, but self-ionization to $[Cp^*MoO_2^+]$ and $[Cp^*MoO_3^-]$ occurs to a larger and larger extent as the water content in the solvent mixture increases. In 20% $MeOH/H_2O$, the compound behaves as a strong electrolyte, affording as the preponderant species $[Cp^*MoO_2^+]$ at pH < 2 and $[Cp^*MoO_3^-]$ at pH $>$ 5. Both species, plus a minor quantity of $[Cp^*MoO_2(OH)]$, are present at intermediate pH values.[25]

The first part of our investigation was devoted to ESI-MS studies of the reactant $[Cp^*_2Mo_2O_5]$ in order to find the analytical conditions that would most closely reflect its speciation in solution. It is worth noting in this respect that ESI-MS provides a sensitivity advantage over the previous analyses, which may have missed some less dominant species. On the other hand, even though ESI-MS is amongst the least intrusive mass spectrometric techniques,[26] the ionization process may nevertheless introduce fragmentation and rearrangement processes resulting in the observation of peaks of species that are not present in the solution. The experimental conditions must therefore be carefully optimized in order to minimize these phenomena. It is also important to verify that no redox process takes place in the ESI chamber in the absence of an applied electrochemical potential. For practical reasons, the ESI-MS studies were conducted in an $MeOH/H_2O$ (1:1) mixture containing a 0.1 M CH_3COONH_4/CH_3COOH buffer at pH = 4. Under these conditions, a substantial amount of dimolybdenum species (either the neutral $[Cp^*_2Mo_2O_5]$ or the tight ion pair $[Cp^*MoO_2^+]$,$[Cp^*MoO_3^-]$) is also present in solution.

Figure 1 compares ESI-MS analyses of a 0.1 mM solution of $[Cp^*_2Mo_2O_5]$ in positive (a) and negative (b) detection modes. The positive-mode ESI-MS spectrum exhibits four major isotopic patterns, corresponding to mono-, di-, tri-, and tetranuclear species, respectively. The mononuclear region shows two major species [see left insert in Figure 1 (a)], both exhibiting the characteristic, seven-peak isotopic pattern of a single Mo atom. The first species is characterized by an isotopic pattern at m/z = 259−267 and corresponds to the $[Cp^*MoO_2^+]$ cation, while the second one, starting 18 m/z units higher (m/z = 277−285), is attributable to the protonated hydroxo species $[Cp^*MoO_3H_2^+]$. While the former is a solution-borne species, the latter results from the protonation of $[Cp^*MoO_2(OH)]$ and $[Cp^*MoO_3^-]$ in the ESI chamber (its pK_a was estimated as ca. −2). Because of this protonation process, the ESI-MS fails to duplicate the known acid-base speciation.[25]

Two major species appear in the dimolybdenum region, both characterized by the expected isotopic distributions for species containing two Mo centers (see second insert of Figure 1 (a)]. The most abundant isotopic pattern is at m/z = 535−551, which corresponds to the protonated form of $[Cp^*_2Mo_2O_5]$. As stated above, this compound exists as a molecular species in organic solvents (including pure MeOH) but it partially dissociates in the presence of water. In an $MeOH/H_2O$ (1:1) mixture, as used in this study, the conductivity investigations showed that part of the dinuclear compound is undissociated. The observed peak can therefore be attributed to the combination of $[Cp^*_2Mo_2O_5]$ with protons originating from the ammonium buffer. The less abundant and lighter pattern (m/z = 517−533) in this region has 18 fewer m/z units than the previous one and is therefore attributable to a dehydrated form. Probably one of the Cp* protons is involved in the process leading to this species, thereby signaling ESI-MS fragmentation.[27,28]

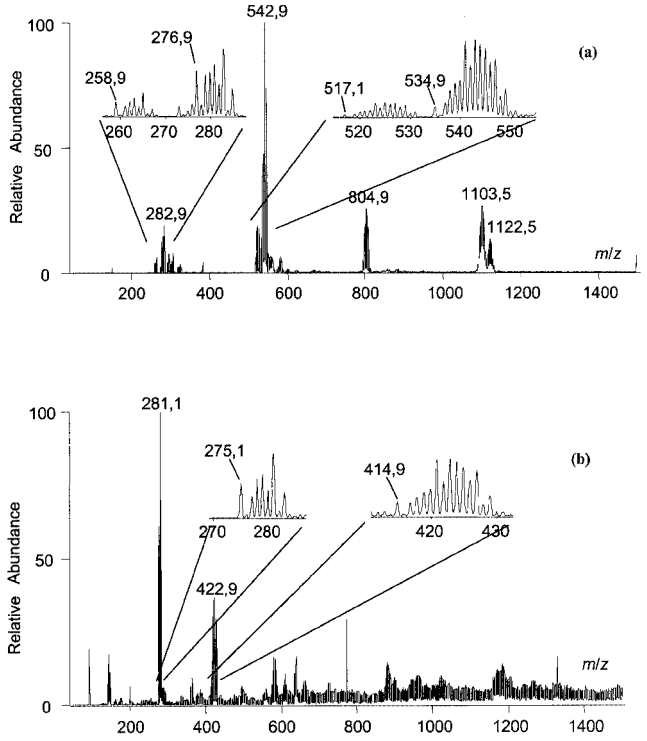

Figure 1. Electrospray mass spectra of a solution of $[Cp^*_2Mo_2O_5]$ (0.1 mM) in H_2O/MeOH (1:1) at pH = 4; heated capillary temperature = 100 °C; (a) positive mode; (b) negative mode; the largest *m/z* peaks are marked in the Figure and the first isotope in each isotopic pattern is marked in the inserts

The isotope patterns at *m/z* = 793−815 and 1090−1117 fit the calculated distributions of $[Cp^*_3Mo_3O_7^+]$ (slope = 1.0005, correlation coefficient R^2 = 0.999) and $[Cp^*_4Mo_4O_{11}H_3^+]$ (slope = 1.008, R^2 = 0.9998), respectively, very well.[29] Thus, both complexes still feature the metal atom in the oxidation state +6. It should be noted that a deviation of a single atomic mass unit (AMU), corresponding to a one-electron reduction process, can easily be distinguished by the isotope distribution fit. For example, curve-fitting of the isotope distribution of a hypothetical $[Cp^*_4Mo_4O_{11}H_4^+]$ to the observed isotope pattern for the tetranuclear species gives a slope of 1.004 but a correlation coefficient R^2 = 0.5451. Of course, the fitting of lower molecular weight molybdenum complexes to the observed patterns is even more sensitive to the assigned composition.

The negative mode spectrum of the same $[Cp^*_2Mo_2O_5]$ solution is given in Figure 1 (b). The major pattern at *m/z* = 275−283 corresponds to the deprotonated mononuclear species $[Cp^*MoO_3^-]$ (left insert). The second major distinguishable pattern (right insert, *m/z* = 415−431) is attributable to a species of formula $[Cp^*Mo_2O_6^-]$: the product of the replacement of one Cp^{*-} group with O^{2-}, a result of ESI-MS fragmentation. The negative mode spectrum also shows a much higher background current, relative to the positive mode spectrum, for *m/z* > 500. For these reasons, all further studies were conducted in the positive ion mode.

Two additional ESI-MS parameters were singled out for further optimization: the temperature of the heated capillary and the heated capillary voltage. Figure 2 (a) shows the ESI-MS spectrum recorded under the same conditions of Figure 2 (a), except that the heated capillary was maintained at 200 °C rather than at 100 °C. The differences between the two spectra confirm that the heated capillary temperature is a decisive factor in ESI-MS studies of our compounds. A comparison between the inserts of Figure 1 (a) and Figure 2 (a) reveals that $[CpMoO_3H_2^+]$ almost completely disappears at high temperatures, while the abundance of a new species with *m/z* = 273−281 (corresponding to $[CpMoO_3H_2^+ - 3\ H]$) − evidently resulting from a fragmentation process − increases. Furthermore, the daughter product with *m/z* = 517−533 in the dinuclear region becomes the preponderant species, while the original isotope pattern of the protonated dinuclear species $[Cp^*_2Mo_2O_5H^+]$ almost completely disappears. In addition,

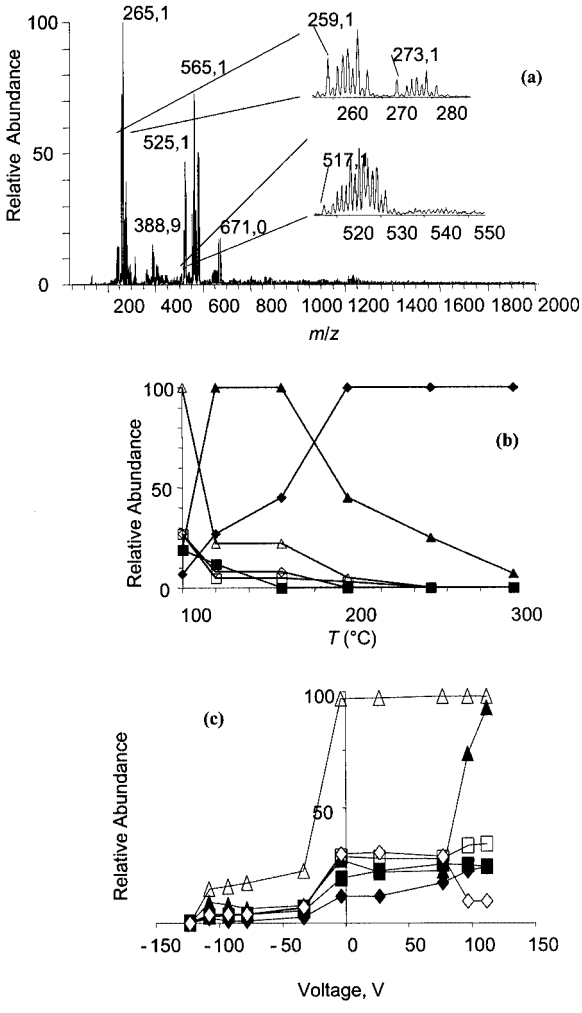

Figure 2. (a) Positive-mode electrospray mass spectra of a solution of $[Cp^*_2Mo_2O_5]$ (0.1 mM) in H_2O/MeOH (1:1) at pH = 4; heated capillary temperature = 200 °C; (b) and (c) evolution of the relative intensity of selected species {black diamonds: $[Cp^*MoO_2^+]$; black squares: $[Cp^*MoO_3H_2^+]$; black triangles: $[Cp^*_2Mo_2O_5H^+ - H_2O]$; white triangles: $[Cp^*_2Mo_2O_5H^+]$; white squares: $[Cp^*_3Mo_3O_7^+]$ species; white diamonds: $[Cp^*_4Mo_4O_{11}H_3^+]$} as a function of the heated capillary temperature (b) and heated capillary voltage (c)

other fragmentation products are also formed in relatively large proportions. Evidently, $[Cp^*_2Mo_2O_5]$ is cleaved at high temperatures.

The temperature dependence demonstrated in Figure 2 (a) is further elaborated upon in Figure 2 (b). The figure shows the dependence of several of the most abundant positive ion peaks as a function of the heated capillary temperature. Peak heights were normalized to the highest peak observed at the given heated capillary temperature. Under increased temperature conditions the abundance of the parent peak of the protonated $[Cp^*_2Mo_2O_5]$ decreases, while the abundance of the secondary peak of the dehydrated moiety goes through a maximum at 120−180 °C and then also decreases. The abundance of the monomeric form $[Cp^*MoO_2^+]$ increases monotonically with temperature, indicating a somewhat surprising thermal stability for this ion, whereas its relative abundance at 100 °C amounts to less than 10% of the dinuclear peak.

The relative abundances of the tri- and tetranuclear molybdenum species decrease steadily with the heated capillary temperature. This decrease suggests that the tri- and tetranuclear molybdenum species originate from the aqueous solution and that they were not generated by condensation reactions in the ESI chamber. Condensation reactions and dehydration should increase at higher temperatures, contrary to the tendency exhibited in Figure 2 (b). We thus believe that these compounds do exist in the solution, although they were not observed before by any other technique. These results directed our subsequent experiments to low source temperatures, set at 100 °C for detector sensitivity reasons.

The capillary voltage value was optimized (+25 V) during the automatic tuning process of our MS in order to give the highest sensitivity for the mass of $[Cp^*_2Mo_2O_5H^+]$. Since prior studies had pointed to the sensitivity of the observed spectra of organometallic complexes to the heated capillary voltage,[30] we carried out a set of tests in order to check the influence of this parameter in our case. The experiments showed that the spectra were not significantly changed as long as the heated capillary voltage remained within the −25 to +100 V range, see Figure 2 (c). It should be pointed out that no reduced molybdenum species were observed even when this potential was set as low as −100 V. Only for more negative cone voltages (< −110 V) did a reduction peak become observable (m/z = 777−799, attributable to $[Cp^*_3Mo_3{}^{V,V,VI}O_6^+]$).

The concentration dependence of the peak intensities for the five major species are shown in Figure 3. The relative abundances of the $[Cp^*MoO_3H_2^+]$ and $[Cp^*MoO_2^+]$ species are virtually concentration-independent, whereas those of all other species, including the dinuclear $[Cp^*_2Mo_2O_5H^+]$, increase with concentration. Given the established equilibrium in MeOH/H_2O solutions of various proportions between the dinuclear $[Cp^*_2Mo_2O_5]$ on one hand, and the separate ions $[Cp^*MoO_2^+]$ and $[Cp^*MoO_3^-]$ on the other, an increase of the relative abundance of dinuclear species with the concentration was to be expected. In principle, the observed increase in relative intensity with concentration for the trinuclear and tetranuclear peaks could be equally well explained by invoking similar solution equilibria. Since we have shown that a water-rich environment favors the spontaneous ionization of $[Cp^*_2Mo_2O_5]$ into $[Cp^*MoO_2^+]$ and $[Cp^*MoO_3^-]$, we propose that the trinuclear species derives from the combination of, for example, $[Cp^*MoO_3^-]$ with two $[Cp^*MoO_2^+]$ ions, as shown in Scheme 1.

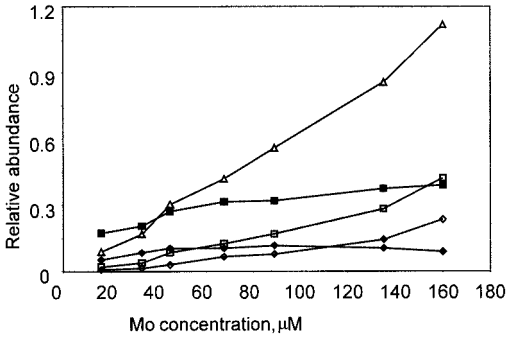

Figure 3. Concentration dependence of the relative intensities of selected species; spectra were recorded under the conditions of Figure 1 (a); black diamonds: $[Cp^*MoO_2^+]$; black squares: $[Cp^*MoO_3H_2^+]$; white triangles: $[Cp^*_2Mo_2O_5H^+]$; white squares: $[Cp^*_3Mo_3O_7^+]$; white diamonds: $[Cp^*_4Mo_4O_{11}H_3^+]$

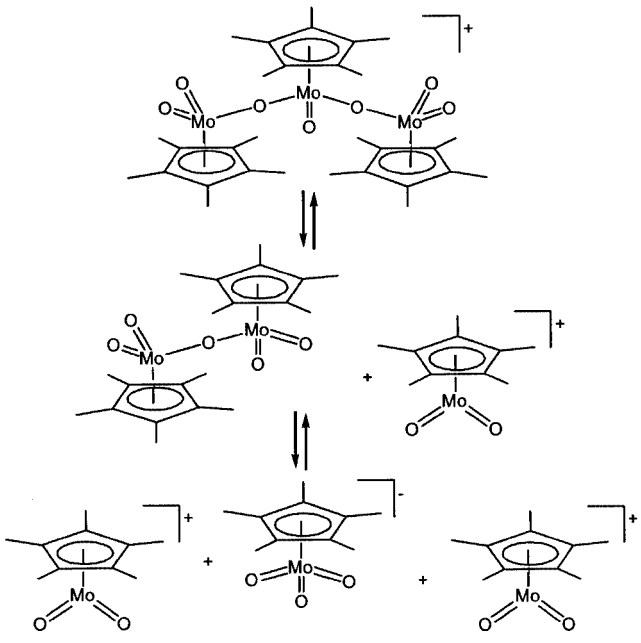

Scheme 1

A similar association process may occur for the tetranuclear species, although a simple breakdown into mononuclear charged components and a tentative structure for the assembled species cannot be as easily imagined as for the trinuclear species. It should further be remarked that these ionic association processes should be favored by the low polarity of the water/methanol (50:50) mixture. In the more polar (80:20) mixture, in which our previous speciation study was conducted,[25] no evidence for the presence of these ions was obtained, although the kinetics and conduc-

tivity may have been insensitive to the presence of small amounts of these species.

The choice of a buffer based on the ammonium cation rather than on other metal cations was dictated by the observation of complicating metal addition processes when the latter were used. For instance, Figure 4 shows the basic set of peaks of the dinuclear species in the presence of 1 M $LiBF_4$ (acidified to pH = 3.3 by acetic acid). Competitive protonation and formation of adducts with metal cations, the latter being preponderant, take place, and both adducts are discerned in the ESI-MS spectrum. The formation of metal ion adducts in preference to protonation in the ESI-MS chamber is a known phenomenon for neutral organometallic molecules.[31,32]

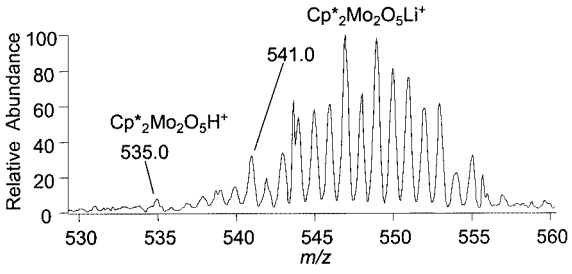

Figure 4. Detailed positive-mode electrospray mass spectra for a 0.1 mM solution of $[Cp^*_2Mo_2O_5]$ in H_2O/MeOH (1:1) in the presence 1 M $LiBF_4$ (pH = 3.3)

In addition to obtaining optimal ESI-MS parameters, two important interim conclusions could be reached on the basis of open-circuit studies of $[Cp^*_2Mo_2O_5]$ in methanol/water/acetate solutions. Firstly, condensation reactions do not occur to a large extent in the ESI chamber; the tri- and tetranuclear molybdenum species appear to be already present in solution. Secondly, reduced molybdenum compounds are not generated to any noticeable extent in the ESI-MS. This condition is a prerequisite for our further on-line electrochemical reduction/ESI-MS studies.

(b) On-Line Electrochemical Reduction/ESI-MS Study

Figure 5 (a) shows the background 3 mV/s voltammogram of an MeOH/H_2O (1:1) solution (acetic buffer, pH = 4) recorded in a regular three-compartment electrochemical cell with a glassy carbon working electrode. Curve (b) shows the voltammogram of a 1 mM solution of $[Cp^*_2Mo_2O_5]$. The reduction wave starts at approximately −0.45 V vs. saturated Ag/AgCl electrode. The current/potential curves at the forward and backward scans nearly coincide and the height of the reduction wave is virtually independent of the scan rate for a fairly wide range of scan rates (3−100 mV/s). The last two observations indicate that the electrochemical reduction of $[Cp^*_2Mo_2O_5]$ is controlled by an interfacial step and it is not diffusion-limited. A slope change at $E = -0.65$ V implies that an additional reduction step is switched on at this potential. It is quite obvious that identification of the electroreduction products solely on the basis of the voltammetric experiment is impossible.

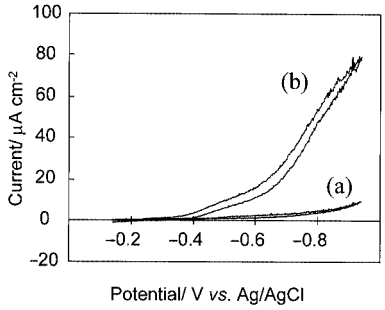

Figure 5. Voltammetry in 0.25 M NH_4Ac in H_2O/MeOH (1:1) at pH = 4 on a GC electrode; scan rate: 3 mV/s; (a) blank solution; (b) 1 mM $[Cp^*_2Mo_2O_5]$

Preparative electrolysis studies at −0.6, −0.7, and −0.8 V with a conventional 10-mm-diameter glassy carbon electrode showed a gradual decrease of the current after prolonged polarization (2 h) due to the formation of a thick oxide film on the electrode surface. This was accompanied by the accumulation of polymeric products in the solution, which increased the turbidity of the solution and could also be detected by ESI-MS studies. We thus preferred to direct our electrochemical studies towards the flow-through configuration because the shorter timescale of the experiment and the constant renewal of the electrolyzed solution insured the absence of contamination from slower secondary reactions.

The electrochemical investigations were therefore pursued in a combined on-line electrochemical cell/ESI-MS experimental setup (Figure 6). The flow configuration and the characteristics of this setup are described in full details elsewhere.[33] Briefly, the feed stream in this cell reaches the sample electrode through the outer annulus of a concentric dual capillary arrangement. The feed stream is split into an outer stream that diverges outwards and washes away the cell solution and an axial stream that flows inward through a 20-μm gap between the glassy carbon sample and the flat end of the dual capillary arrangement. The feed converges into an inner capillary transfer line that leads to the mass spectrometer. We preferred this type of setup over a regular tabular flow cell in order to avoid chemical interference due to the oxidation reactions on the counter-electrode. This configuration also minimizes ohmic potential drops in the cell. Note that, unlike regular flow-through electrochemical detectors that operate under mass-transport-limited conditions, we target a kinetically controlled reaction. Thus, by use of conventional flow-through cells, oxidized compounds generated at the counter-electrode will most probably escape electroreduction on the working electrode and will reach the transfer line to the mass spectrometer. This phenomenon may result either in the appearance of oxidized species in the MS or, even worse, in the occurrence of chemical reactions between the compounds generated at the counter-electrode and the working electrode. The flow cell of Figure 6 assures the confinement of the compounds gen-

erated at the counter-electrode away from the transfer line to the mass spectrometer.

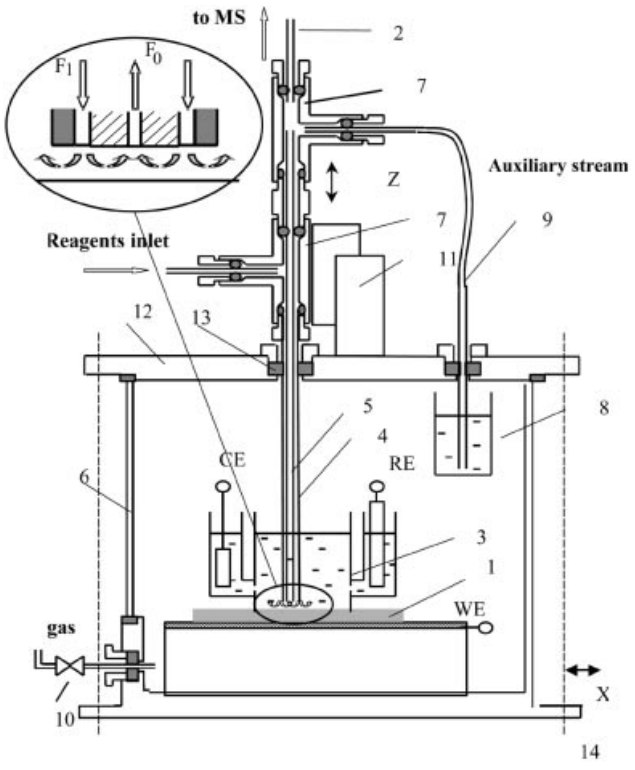

Figure 6. Scheme of the electrochemical cell used in this study; 1: working electrode; 2: transfer line to the ESI/MS; 3: three-compartment electrochemical glass cell; 4: outer capillary; 5: inner capillary; 6: pressure chamber; 7: T-junction; 8: auxiliary fluid beaker; 9: auxiliary capillary; 10: pressure regulator; 11: Z-translation stage; 12: pressure chamber cover; 13: rubber seal; 14: steel rod; insert: a scheme of the miniature flow cell formed at the bottom of the coaxial capillary setup; F_1 is the feed through the annulus of the coaxial capillary setup; F_0 is the product stream to the MS

Mass spectra are continuously recorded during the coupled EC/ESI-MS experiments, and so a three-dimensional domain of signal intensities as a function of *m*/*z* and time is generated. Projection of this space onto an *m*/*z* axis for a given time range gives a time-integrated traditional mass spectrum, while projection onto the time axis for a given *m*/*z* range gives the time evolution of the chosen species. Under potential ramp constraint, a potential-dependent generation or consumption of the specific compounds is obtained.

In order to translate the time-dependent relative abundances into potential-dependent curves it is necessary to measure the lag time in the transfer line from the electrochemical flowcell to the mass spectrometer and to estimate the degree of back-mixing (i.e. signal averaging) in the transfer line. These parameters were determined by application of a potential step to the GC working electrode between −0.35 and −0.9 V. According to the voltammetric curve (b) shown in Figure 5, the Mo species in the solution are exclusively in their oxidized state at $E = -0.35$ V, while reduction processes occur at $E = -0.9$. Figure 7 shows that the application of the potential step sharply decreases the concentration of $[Cp^*_2Mo_2O_5H^+]$. The intensity of the signal starts to decrease after a delay time of ca. 25 s. This seemingly corresponds to the retention time in the transfer line, in agreement with flow calculations. An additional 15-s interval is required to reach the half height of the concentration step change. The deviation of the MS response from a sharp step change is attributable to back-mixing in the transfer line and to the time constant of the ESI interface. Thus, the "lag time" of the instrument is approximately 40 s. The coupled EC/ESI-MS experiment with a continuous potential linear scan were therefore recorded under the quite slow scan rate conditions of 0.5 mV s^{-1}.

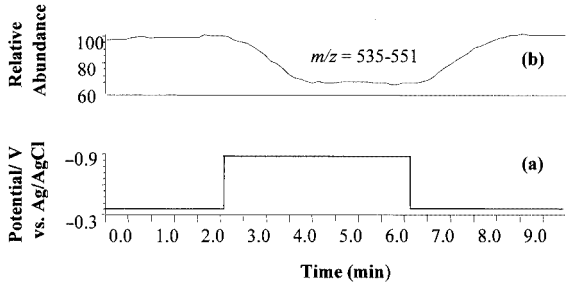

Figure 7. Response of the EC/ESI-MS (positive mode) to a potential step change of the GC electrode; feed stream: $[Cp^*_2Mo_2O_5]$ (1 mM) in 0.25 M NH_4Ac H_2O/MeOH (1:1) at pH = 4; (a) potential step function; (b) time trace of the $[Cp^*_2Mo_2O_5H^+]$ signal intensity, integrated over the given *m*/*z* range

Figure 8 shows the potential-dependent abundance of all major species present in solution under open-circuit conditions {i.e., the mononuclear $[Cp^*MoO_2^+]$ and $[Cp^*MoO_3H_2^+]$, the dinuclear $[Cp^*_2Mo_2O_5H^+]$, the trinuclear $[Cp^*_3Mo_3O_7^+]$ and the tetranuclear $[Cp^*_4Mo_4O_9(OH)_3^+]$; see Figure 1 (a)}, during the electroreduction process. The recorded signal was obtained by summing the relative abundances of all the peaks in each respective *m*/*z* range, covering the entire isotope envelope. The time axis of the product evolution curve was synchronized with the corresponding potential scale by the use of a 40 s delay time based on the potential step-change studies. During the backward, anodic scan, the concentration profiles essentially follow the same pattern as observed in the cathodic scan, indicating that the experiment is not significantly polluted by film-deposition processes. It is to be noted that all species start to be reduced at approximately the same potential. This would seem consistent with the presence of rapid equilibria between the various complexes, as proposed above, and with the selective reduction of only one of these species. However, it cannot be excluded that all the different species, or at least some of them, are reduced independently at approximately the same potential. A clarification of this point needs additional experiments under different concentration and pH conditions, which are in progress and will be reported in due course.

The mass spectrum measured at the switching potential (see Figure 9) reveals a set of new peaks corresponding to the different products of electrochemical reduction. New isotopic patterns corresponding to the formation of reduced

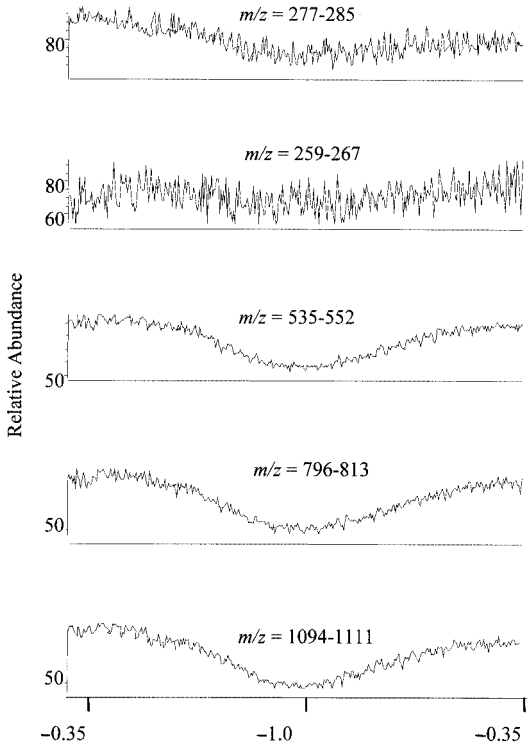

Figure 8. Mass spectra and potential-dependent abundance of the initially present species during a linear potential sweep (scan rate 0.5 mV s^{-1} from −0.35 to −1.0 V and back); experimental conditions are as specified in Figure 7

mononuclear, dinuclear, trinuclear, and tetranuclear species evolved at reduced potentials.

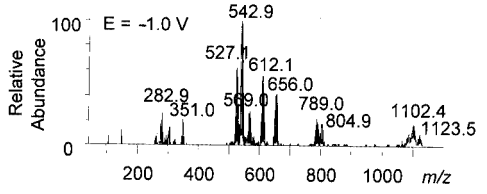

Figure 9. Mass spectrum recorded at $E = -1.0$ V (switching potential) during the EC/ESI-MS study of $[Cp^*_2Mo_2O_5]$; experimental conditions are as specified in Figure 7

The potential-dependence of the MS intensities of the reduced molybdenum species are shown in Figure 10, together with their corresponding MS isotopic patterns and assigned structures. The last are based on the fit of the observed MS isotope patterns to the calculated isotope distributions. It should be noted that, although the molecular weight and Mo nuclearity are unambiguous, the assigned structures are only tentative. Alternative possibilities exist: species $[Cp^*_2Mo_2O_2(OAc)_2^+]$, for instance, may display two terminal oxo and two bridging acetato ligands, or two bridging oxo and two terminal (chelating) acetato ligands, or all ligands may be bridging, as shown in Figure 10. The chosen assignments are based on comparison with related examples from the literature. The closest analogues to the dinuclear complexes are half-sandwich sulfido and alkylsulfido species extensively investigated in the groups of Rakowski-Dubois and Pétillon.[34−36] No previous report of compounds in which the $[Cp^*_2Mo_2^{n+}]$ core is fully coordinated by hard, oxygen-based ligands seems to be available, the exceptions being the starting material $[Cp^*_2Mo_2O_5]$ and the corresponding Mo^V dimer $[Cp^*_2Mo_2O_4]$.[24,37,38] Related trinuclear [Cp*Mo] species of formula $[Cp^*_3Mo_3O_6H_n]^{2+}$ (n = 4, 5, 6), on the other hand, have previously been reported by Bottomley et al.[39] Amongst tetranuclear oxo clusters, the closest relationship is found with a Cp derivative, a red isomer of "$[CpMoO_2]$", the nuclearity of which was based solely on molecular weight determinations.[40] The more stable orange isomer has a dinuclear structure. A more reduced tetranuclear oxo cluster, $[Cp^*_4Mo_4O_7]$, formally a $Mo^{4.5+}$ species, has also previously been described.[41] No indication has been obtained, however, that the latter species is formed under our experimental conditions.

As shown in Figure 10 (central column), the isotopic envelopes of most identified species do not overlap with the other nearby isotopic patterns. An exception is the dinuclear complex $[Cp^*_2Mo_2O_4H^+]$ (m/z = 519−535), which overlaps with another species with m/z = 517−533, a daughter ion obviously deriving from hydrogen loss from the Cp* rings. The voltage-dependent intensity of the $[Cp^*_2Mo_2O_4H^+]$ species is obtained by integration of an m/z region where the overlap with the minor species is minimal (m/z = 532−534). Complex $[Cp^*MoO(OAc)^+]$ (m/z = 302−310) overlaps with another species with one fewer mass unit, indicating fragmentation with loss of hydrogen atoms. The envelope of the reduced trinuclear species is shifted to lower m/z by exactly 16 units from that of its precursor complex $[Cp^*_3Mo_3O_7^+]$, suggesting its formulation as a proton-free hexaoxo species.

The assignment of the chemical formulas for the reduced species is further supported by ion-trap MS^n fragmentation studies, the results being collected in Table 1. All MS^n studies were conducted with isolation widths corresponding to the whole range of the observed isotope patterns. The m/z = 302−310 monoacetate complex shows loss of acetic acid and formation of a methanol adduct in the MS^2. Similarly, the diacetate mononuclear complex (m/z = 345−353) exhibits loss of an acetic acid unit. The low stability of these low-weight mononuclear fragments did not allow further MS^3 fragmentation studies. The assignment of the m/z = 519−535 to a $[Cp^*_2Mo_2O_4H^+]$ species is supported by $MS^2/MS^3/MS^4$ subsequent fragmentations showing a consecutive series of single dehydrations. In addition, an MS^n study of separately synthesized $[Cp^*_2Mo_2O_4]$ revealed an identical fragmentation pathway. The assignment of m/z = 561−577 to a $[Cp^*_2Mo_2O_3(OAc)]$ species is supported by MS^2 fragmentation showing neutral losses of an acetyl fragment or water. The isotope pattern at m/z = 604−620 is assigned to $[Cp^*_2Mo_2O_2(OAc)_2^+]$ on the basis of the acetyl loss and dimer cleavage to give the $[Cp^*MoO_2(OAc)^+]$ and $[Cp^*MoO(OAc)_2^+]$ cationic fragments in the MS^2. The $[Cp^*_2Mo_2O(OAc)_3^+]$ complex (m/z = 647−663) gives rise to three different fragmentations at different collision ener-

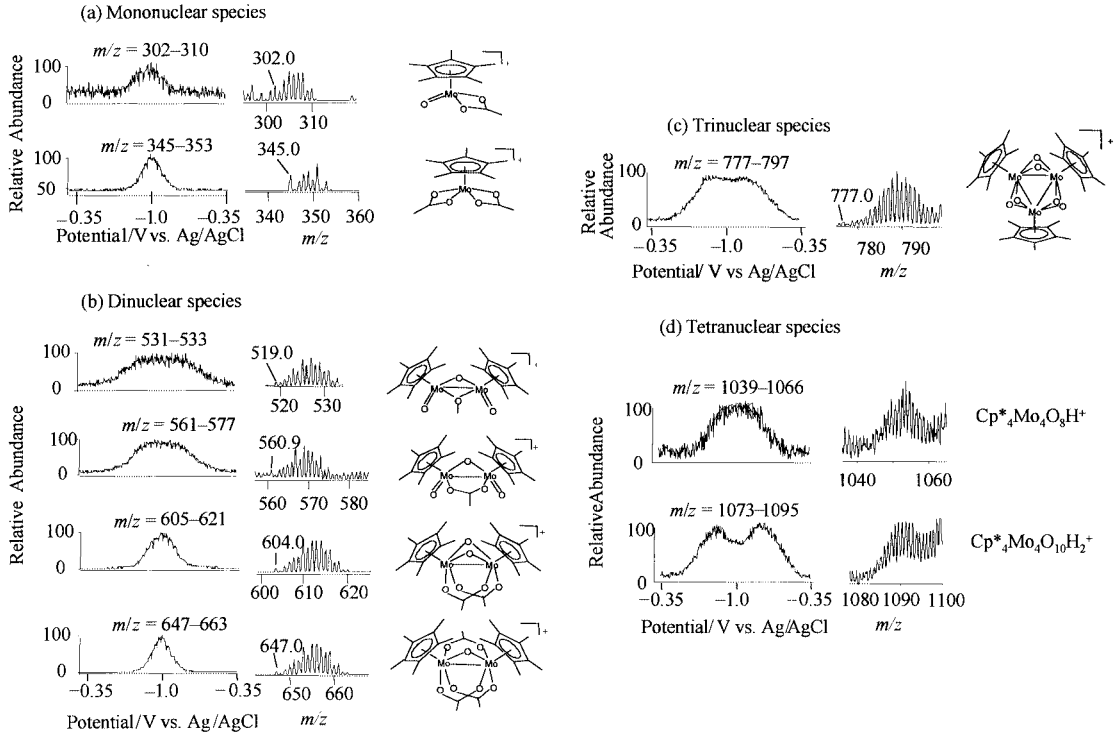

Figure 10. Potential dependence of the relative abundance of selected species generated during the coupled electrochemistry/ESI-MS of $[Cp^*_2Mo_2O_5]$; left: potential-dependent evolution of the integrated signal, the *m/z* range used for signal integration is specified above each curve; center: expanded isotopic pattern; right: proposed chemical structure; experimental conditions are as specified in Figure 7

gies, corresponding to loss of a one and two acetyl groups, and to dimer cleavage to give the mononuclear fragment $[Cp^*Mo(OAc)_2^+]$. Further MS^3 fragmentation of $[Cp^*Mo(OAc)_2^+$ reveals an additional acetyl loss. Finally, MS^4 fragmentation of $[Cp^*Mo(OAc)^+]$ reveals one oxygen atom loss.

The MS^n fragmentation of the trinuclear species is even more complicated. The primary species $[Cp^*_3Mo_3O_6^+]$ (m/z = 777−799) produces four fragments in the MS^2. The first two correspond to loss of $C_5Me_4CH_2$ and $C_5Me_4CH_2 + H_2O$, respectively, the third is a methanol adduct of the second, and the fourth corresponds to $[Cp_2Mo_2O_4^+]$, resulting from the loss of $[Cp^*MoO_2]$. It should be noted that the latter cleavage involves disruption of two oxo bridges and indeed it occurs at much higher collision energy than the first three processes. MS^3 fragmentation of the methanol adduct results in MeOH loss, and a subsequent MS^4 fragmentation reveals four ions corresponding to Cp* loss plus formation of three solvent adducts of the resulting fragment. MS^3 and MS^4 fragmentation of $[Cp^*_2Mo_2O_4^+]$ give rise to subsequent dehydration processes. No MS^n study of the reduced tetranuclear species could be carried out, because of the very low abundance of these peaks.

Table 2 presents the approximate potential values for the appearance of the various reduced species that may be measured in Figure 10. Analysis of these values enabled us to derive a certain number of conclusions: (i) for a given nuclearity, the potential becomes more negative as the oxidation state decreases, as one would expect, (ii) when comparing species of the same formal oxidation state, the dinuclear compounds are always obtained at a less negative potential than the mononuclear ones, while the tetranuclear $[Cp^*_4Mo_4O_8H^+]$ species is obtained at approximately the same potential (−0.52 V) as the dinuclear $[Cp^*_2Mo_2O_4H^+]$ species (−0.48 V), (iii) the latter complex is obtained at a less negative reduction potential than the other Mo^V dinuclear species containing an acetate ligand, and finally (iv) this potential nearly matches the potential at which the peaks of the starting complex start to disappear (Figure 8). The large deviation between the threshold formation potentials and the mid-intensity potential $E_{1/2}$ points to kinetically controlled formation reactions for all of the reduced molybdenum species. This is unfortunate, since it precludes direct evaluation of the corresponding thermodynamic formation parameters for these new compounds.

These combined observations may be interpreted as follows. The mononuclear products are likely to derive from the one-electron reduction of $[Cp^*MoO_2^+]$, affording a neutral radical. At more negative potentials, the latter species may be reduced further, possibly after a protonation stage. At each oxidation state level, two competing processes may occur: namely acetate/hydroxide exchange and dimerization (accompanied by the establishment of a metal−metal bond). For instance, the neutral Mo^V intermediate may dimerize to $[Cp^*_2Mo_2O_4]$, which is then detected by ESI-MS in its protonated form, or it may be protonated and the resulting $[Cp^*MoO(OH)^+]$ species may undergo a hydroxide/acetate exchange to produce the observed

Table 1. Assigned formulas and MS^n studies of the reduction products formed during EC/ESI-MS studies of $[Cp^*_2Mo_2O_5]$

Product of EC reduction	MS^2		MS^3		MS^4	
Loss	Range of isotopic pattern	Loss	Range of isotopic pattern	Loss	Range of isotopic pattern	
$[Cp^*_3Mo_3^{V,V,VI}O_6^+]$	$-C_5Me_4CH_2$	643–665	n.a.[a]	n.a.	n.a.	n.a.
m/z = 777–799						
$-Cp^*-OH$	625–647	n.a.	n.a.	n.a.	n.a.	
$-Cp^*-OH+MeOH$	653–675	$-MeOH$	625–647	$-H_2O$	607–629	
$-C_5Me_4CH_2+2H_2O$	509–531					
$-C_5Me_4CH_2+2H_2O+MeOH$	541–563					
$-C_5Me_4CH_2+H_2O$	490–512					
$[Cp^*_2Mo_2^{IV,IV}O(OAc)_3^+]$	$-OAc-O$	572–588	n.a.	n.a.	n.a.	n.a.
m/z = 647–663						
$-2(OAc)-O$	513–529	n.a.	n.a.	n.a.	n.a.	
$-[Cp^*MoO(OAc)]$	345–353	$-OAc$	286–294	$-O$	270–278	
$[Cp^*_2Mo_2^{IV,V}O_2(OAc)_2^+]$	$-OAc$	542–558	n.a.	n.a.	n.a.	n.a.
m/z = 604–620						
$-[Cp^*MoO(OAc)]$	302–310	n.a.	n.a.	n.a.	n.a.	
$-[Cp^*MoO]$	361–369	n.a.	n.a.	n.a.	n.a.	
$-2(OAc)$	486–502	$-H_2O$	468–484	n.a.	n.a.	
$[Cp^*_2Mo_2^{V,V}O_3(OAc)^+]$	$-OAc$	502–518	n.a.	n.a.	n.a.	n.a.
m/z = 561–577						
$-H_2O$	543–559	n.a.	n.a.	n.a.	n.a.	
$[Cp^*_2Mo_2^{V,V}O_4H^+]$	unclear	360–368	n.a.	n.a.	n.a.	n.a.
m/z = 519–533						
$-H_2O$	501–517	$-H_2O$	483–499	$-H_2O$	465–481	
$[Cp^*Mo^{IV}(OAc)_2^+]$	$-AcOH$	285–293	n.a.	n.a.	n.a.	n.a.
m/z = 345–353						
$[Cp^*Mo^{V}O(OAc)^+]$	$-AcOH+MeOH$	274–282	n.a.	n.a.	n.a.	n.a.
m/z = 302–310						

[a] n.a. = not available

Table 2. Threshold potential (E_{in}) and half-wave potential ($E_{1/2}$) corresponding to the formation of reduced compounds during the EC/ESI-MS study of $[Cp^*_2Mo_2O_5]$ in methanol/water/acetate solutions; experimental conditions are described in the caption of Figure 9

Compound	m/z	E_{in}[a] [V]	$E_{1/2}$ [V]
$[Cp^*_4Mo_4^{V,VI,VI,VI}O_{10}H^+]$	1073–1100	−0.40	−0.47
$[Cp^*_4Mo_4^{V,V,V,V}O_8H^+]$	1040–1067	−0.52	−0.61
$[Cp^*_3Mo_3^{V,V,VI}O_6^+]$	777–800	−0.48	−0.75
$[Cp^*_2Mo_2^{IV,IV}O(OAc)_3^+]$	647–663	−0.78	−0.94
$[Cp^*_2Mo_2^{IV,V}O_2(OAc)_2^+]$	604–620	−0.74	−0.91
$[Cp^*_2Mo_2^{V,V}O_3(OAc)^+]$	561–577	−0.55	−0.81
$[Cp^*_2Mo_2^{V,V}O_4H^+]$	519–533	−0.48	−0.77
$[Cp^*Mo^{IV}(OAc)_2^+]$	345–353	−0.81	−0.94
$[Cp^*Mo^{V}O(OAc)^+]$	302–310	−0.76	−0.92

[a] E_{in} is defined as the potential corresponding to a 100% abundance increase over the background signal. $E_{1/2}$ = potential at which half of the maximum signal intensity is obtained.

$[Cp^*MoO(OAc)^+]$. The driving force of the rapid and irreversible metal–metal bond formation would account for the smaller reducing potential needed to generate an oligonuclear species relative to a mononuclear one at the same oxidation state level. It is also possible, however, that the higher nuclearity products are obtained by direct reduction of the higher nuclearity species present in solution. It can be noted that each one-electron reduction for the mononuclear and dinuclear species is formally accompanied by the replacement of one oxygen atom with an acetate group (corresponding to a mass increase of 43 units). The only exception to this substitution rule is the observation of two different compounds with the $Mo_2^{V,V}$ core and related to each other by the formal replacement of an OH with an acetate group. The spectrum in Figure 9 does not show any mononuclear species with a mass greater than the 345–353 envelope, nor dinuclear species with a mass greater than the 647.0–664.0 envelope. This suggests that no Mo species in oxidation states lower than +4 are produced under the experimental conditions chosen.

The major trinuclear product obtained under reducing conditions is an $Mo_3^{V,V,VI}$ species. On the other hand, the same basic structure was reported for the dicationic $Mo_3^{IV,IV,V}$, $Mo_3^{IV,IV,IV}$, and $Mo_3^{III,IV,IV}$ complexes $[Cp^*_3Mo_3O_6H_n^{2+}]$ (n = 4, 5, 6).[39] Although the isotope envelope simulation quite clearly indicates the nature of the major product, minor amounts of products of further reduction cannot be excluded. We did not observe any signals attributable to dicationic species. It is possible that the reduction potential range and the conditions used in this study do not allow access to the more reduced known trinuclear species, which were in fact previously obtained by zinc reduction of $[Cp^*MoO_2Cl]$ under non-aqueous conditions.[39]

As far as the tetranuclear reduction products are concerned, the $[Cp^*_4Mo_4O_8H]^+$ species may be related to the kinetic isomer previously identified for the Cp system when complex $[CpMoCl_4]$ is hydrolyzed, namely $[Cp_4Mo_4O_8]$.[40]

It is believed that this complex does not contain metal−metal bonds, whereas the dinuclear $[Cp_2Mo_2O_4]$ isomer does.[42] The formation of this tetranuclear compound from precursors that themselves are devoid of metal−metal interactions is therefore to be expected. The mixed-valence $[Cp^*_4Mo_4O_{10}H_2]^+$ species does not have any equivalent in the literature. The shape of the abundance vs. potential curve indicates that a direct reduction to other species, possibly the tetranuclear Mo^V cluster, becomes more favorable at more negative potentials.

As clearly shown by the cone voltage optimization study [Figure 2 (c)], the experimental conditions of the positive-mode electrospray process cannot, by themselves, induce an oxidation state decrease for the analyte. The reduced molybdenum products shown in Figure 10 must therefore originate from the electrochemical reactions in the electrochemical cell. The simple chemical composition of these species and the fact that they contain unfragmented acetate and pentamethylcyclopentadienyl ligands lead us to believe that they are all indeed solution-borne species.

Conclusion

The coupled EC/ESI-MS technique has proven to be a powerful analytical tool for the investigation of complex electrochemical transformations. At least six previously unreported species have been identified from the electroreduction of $[Cp^*_2Mo_2O_5]$, and the potential required for the generation of each one has been assessed. These species may be described as oxo- and/or acetate-stabilized $[Cp^*Mo^{n+}]$, $[Cp^*_2Mo_2^{n+}]$, $[Cp^*_3Mo_3^{n+}]$, and $[Cp^*_4Mo_4^{n+}]$ complexes. These species, as well as analogues with less coordinating anionic ligands, may be expected to result in new aqueous coordination chemistry, catalysis, and electrocatalysis. Indeed, a few dinuclear and trinuclear species related to those observed by this EC/ESI-MS investigation have been synthesized and isolated in one of our laboratories. These investigations are described in separate publications.[43,44]

Experimental Section

General Remarks: The starting compound was prepared by a literature procedure.[24] Unless otherwise stated, all solutions were prepared in H_2O/MeOH (1:1) containing CH_3COONH_4 (0.25 M) and buffered to pH = 4.0 by the addition of CH_3COOH. A lower concentration of MeOH in the spray solution resulted in significant losses of relative abundances. All reagents were purchased from Aldrich. Methanol was purchased from Baker and was of HPLC grade. The water was triple-distilled.

Electrospray Mass Spectrometry: A Finnigan (San Jose, USA) LCQ quadrupole ion trap mass spectrometer, equipped with an electrospray ionization (ESI) interface, was used for data acquisition. ESI was operated either in positive or in negative ion mode. In negative mode the tip of the capillary and the sampling cone were maintained at potentials of −3.5 kV (spray voltage) and −70 V (capillary voltage), respectively. In positive mode the spray voltage was at 3.6 kV and the capillary voltage was 25 V. The source temperature was the subject of a separate study. Mass spectra were acquired by scanning the mass analyzer from m/z = 100 to 2000 with five total microscans. The maximum injection time into the ion trap was 50 ms, and the sample injection flow rate was 5 μL min^{-1}. In all experiments, helium was introduced at an estimated pressure of 1 mTorr to improve the ion trapping efficiency. During MS^n experiments the compounds were isolated in the ion trap with isolation width of isotope pattern and activated by use of increased collision energy.

Electrochemical Investigations: A PARC 273 potentiostat/galvanostat (Princeton, USA) was used. A three-compartment electrochemical cell with a disk glassy-carbon working electrode (Metrohm, Herisau, Switzerland), platinum counter-electrode and Ag/AgCl (satd.) reference electrode (Metrohm) was used for the voltammetric studies.

Coupled Electrochemistry/Electrospray Mass Spectrometry: Figure 6 shows a scheme of the experimental setup used in this study; a detailed description of the electrochemical setup is given elsewhere.[33] The setup comprises a three-compartment electrochemical cell placed in a pressure chamber, a two coaxial capillary set, a micropositioning device, and a mass spectrometer equipped with an electrospray ionization (ESI) interface. The working glassy-carbon electrode (1) was pressed to the bottom opening of a three-compartment electrochemical cell (3). A Pt wire counter-electrode and Ag/AgCl (KCl satd.) reference electrodes were placed in the side compartments of the cell. All reported potentials are given relative to this reference electrode. The electrolyte in the cell was 0.25 M CH_3COONH_4 in H_2O/MeOH (1:1), buffered to pH = 4.0 by CH_3COOH. A $[Cp^*_2Mo_2O_5]$ solution (1 mM) in the same electrolyte was pumped through the annulus of the capillary set to the electrode. A coaxial capillary set (4, 5) was used to deliver the reagent solution to the electrode and to transfer the product stream to the interface of the mass spectrometer through the inner capillary. A syringe pump was used to deliver the feed stream to a T-junction (7) located outside the pressure chamber (6), from which the stream was directed through the annulus between the two capillaries to the electrode. The product stream (F_0) was pumped, following the interaction with the electrode, upward through the inner capillary (4) by the excess pressure in the pressure vessel. All capillaries were fused silica from SGE (Austin, USA). The inner capillary was 25 μm inner diameter, 285 μm outer diameter, 15 cm long. The product stream was diluted with excess methanol delivered from a glass beaker (8). The liquid flow rates and dilution ratio (product stream/methanol) were controlled by setting the pressure in the pressure vessel and choice of capillary length and inner diameter. The cell pressure was 2600 kPa. After mixing with the auxiliary liquid, the sample stream was delivered to the ESI interface of the mass spectrometer by a 30 cm long, 50 μm inner diameter capillary. The flow rate of the product stream was ca. 0.7 μL min^{-1}. The methanol flow in the auxiliary capillary was 14 μL min^{-1}. The reagent flow rate (F_1) was set to 4 μL min^{-1}.

Acknowledgments

R. P. and M. V. thank the CNRS and the Ministry of Research for funding. D. S. thanks the Conseil Régional de Bourgogne for a postdoctoral fellowship. A. D. M. and O. L. acknowledge the financial support of the Israel Science Foundation. J. G. thanks the University of Bourgogne for a visiting professorship. We are grateful to the French Embassy in Israel for an Arc-en-Ciel/Keshet travel grant and to Prof. G. Tsirlina for useful discussions.

[1] M. Yamashita, J. B. Fenn, *J. Phys. Chem.* **1984**, *88*, 4451−4459.
[2] R. E. March, R. J. Hujhes, *Quadrupole Storage Mass Spectrometry in Chemical analysis* (Ed.: J. D. Wiefordner), J. Wiley and Sons, New York, **1989**.
[3] M. L. Vestal, *Mass Spectrom. Rev.* **1983**, *2*, 447−480.
[4] W. Henderson, B. K. Nicholson, L. J. McCaffrey, *Polyhedron* **1998**, *17*, 4291.
[5] G. Wolfbauer, A. M. Bond, D. R. MacFarlane, *J. Chem. Soc., Dalton Trans.* **1999**, 4363−4372.
[6] A. M. Bond, R. Colton, D. G. Humphrey, P. J. Mahon, G. A. Snook, V. Tedesco, J. N. Walter, *Organometallics* **1998**, *17*, 2977−2985.
[7] B. Bittins-Cattaneo, E. Cattaneo, P. Konigshoven, W. Vielstich, in *Electroanalytical Chemistry*, vol. 16 (Ed.: A. J. Bard), Marcel-Dekker, New York − Basel − Hong Kong, **1991**.
[8] X. Xu, W. Lu, R. B. Cole, *Anal. Chem.* **1996**, *68*, 4244−4253.
[9] W. Lu, X. Xu, R. B. Cole, *Anal. Chem.* **1997**, *69*, 2478−2484.
[10] A. M. Bond, R. Colton, A. D'Agostino, A. J. Downard, J. C. Traeger, *Anal. Chem.* **1995**, *67*, 1691−1695.
[11] F. Zhou, G. J. Van Berkel, *Anal. Chem.* **1995**, *67*, 3643−3649.
[12] H. Deng, G. J. Van Berkel, *Anal. Chem.* **1999**, *71*, 4284−4293.
[13] D. K. Walanda, R. C. Burns, G. A. Lawrance, E. I. von Nagy-Felsobuki, *J. Chem. Soc., Dalton Trans.* **1999**, 311−321.
[14] B. Salignac, S. Riedel, A. Dolbecq, F. Secheresse, E. Cadot, *J. Am. Chem. Soc.* **2000**, *122*, 10381−10389.
[15] M. Herberhold, W. Kremnitz, A. Razavi, H. Schöllhorn, U. Thewalt, *Angew. Chem. Int. Ed. Engl.* **1985**, *24*, 601−602.
[16] K. Isobe, S. Kimura, Y. Nakamura, *J. Organomet. Chem.* **1987**, *331*, 221−228.
[17] P. Gomez-Sal, E. de Jesus, P. Royo, A. Vazquez de Miguel, S. Martinez-Carrera, S. Garcia-Blanco, *J. Organomet. Chem.* **1988**, *353*, 191−196.
[18] P. Leoni, M. Pasquali, L. Salsini, C. di Bugno, D. Braga, P. Sabatino, *J. Chem. Soc., Dalton Trans.* **1989**, 155−159.
[19] A. L. Rheingold, J. R. Harper, *J. Organomet. Chem.* **1991**, *403*, 335−344.
[20] J. W. Faller, Y. Ma, *J. Organomet. Chem.* **1988**, *340*, 59−69.
[21] K. Umakoshi, K. Isobe, *J. Organomet. Chem.* **1990**, *395*, 47−53.
[22] J. Sundermeyer, U. Radius, C. Burschka, *Chem. Ber.* **1992**, *125*, 2379−2384.
[23] M. S. Rau, C. M. Kretz, G. L. Geoffroy, A. L. Rheingold, *Organometallics* **1993**, *12*, 3447−3460.
[24] D. Saurenz, F. Demirhan, P. Richard, R. Poli, H. Sitzmann, *Eur. J. Inorg. Chem.* **2002**, 1415−1424.
[25] E. Collange, J. Garcia, R. Poli, *New J. Chem.* **2002**, *26*, 1249−1256.
[26] J. C. Traeger, *Int. J. Mass Spectr.* **2000**, *200*, 387−401.
[27] R. Colton, J. C. Traeger, *Inorg. Chim. Acta* **1992**, *201*, 153−155.
[28] A. M. Bond, R. Colton, J. B. Cooper, J. C. Traeger, J. N. Walter, D. M. Way, *Organometallics* **1994**, *13*, 3434−3441.
[29] M. J. Winter, *Sheffield Chemputer*, http://www.shef.ac.uk/chemistry/chemputer/
[30] W. Henderson, J. S. McIndoe, B. K. Nicholson, P. J. Dyson, *Chem. Commun.* **1996**, 1183.
[31] W. Z. Shou, R. F. Browner, *Anal. Chem.* **1999**, *71*, 3365−3373.
[32] E. C. Kempen, J. S. Brodbelt, *Anal. Chem.* **1999**, *71*, 5493−5500.
[33] A. D. Modestov, S. Srebnik, O. Lev, J. Gun, *Anal. Chem.* **2001**, *73*, 4229−4240.
[34] M. Rakowski DuBois, *Chem. Rev.* **1989**, *89*, 1−9.
[35] M. Rakowski DuBois, *Polyhedron* **1997**, *16*, 3089−3098.
[36] F. Y. Pétillon, P. Schollhammer, J. Talarmin, K. W. Muir, *Coord. Chem. Rev.* **1998**, *178/179*, 203−247.
[37] H. Arzoumanian, A. Baldy, M. Pierrot, M. Petrignani, *J. Organomet. Chem.* **1985**, *294*, 327−331.
[38] E. de Jesus, A. Vazquez de Miguel, P. Royo, A. M. M. Lanfredi, A. Tiripicchio, *J. Chem. Soc., Dalton Trans.* **1990**, 2779−2784.
[39] F. Bottomley, J. Chen, K. F. Preston, R. C. Thompson, *J. Am. Chem. Soc.* **1994**, *116*, 7989−7995.
[40] M. Cousins, M. L. H. Green, *J. Chem. Soc.* **1964**, 1567−1572.
[41] F. Bottomley, V. Sanchez, R. C. Thompson, O. O. Womiloju, Z. Q. Xu, *Can. J. Chem.* **2000**, *78*, 383−394.
[42] C. Couldwell, K. Prout, *Acta Crystallogr., Sect. B* **1978**, *34*, 933−934.
[43] F. Demirhan, J. Gun, O. Lev, A. Modestov, R. Poli, P. Richard, *J. Chem. Soc., Dalton Trans.* **2002**, 2109−2111.
[44] F. Demirhan, P. Richard, R. Poli, *Inorg. Chim. Acta*, in press.

Received June 19, 2002
[I02336]